CHAPTER- V

CORRELATION STUDIES

5.1 INTRODUCTION

The dynamic response analysis of any deposit (soil/waste) subjected to cyclic loads caused by earthquakes, explosions, etc. is primarily determined by the stiffness and damping properties of the deposit. The shear strain of greater magnitude is typically involved in earthquake-related problems. In this chapter, some typical correlations and equations are proposed through the dynamic test results discussed in chapter IV for unreinforced and fiber-reinforced MSW fines. The data from the consolidated undrained cyclic triaxial test (excess pore water pressure ratio, dynamic shear modulus, and damping ratio) and the bender element test (small-strain shear modulus) has been used for the correlation studies.

5.2 PORE WATER PRESSURE RATIO (r_u) MODEL FOR FIBER-REINFORCED MSW FINES

Various ru models proposed for soils can be grouped based on stress, strain, energy, plasticity theory, etc. (Prevost,1985; Green et al., 2000; Kokusho, 2013; Adampira and Derakhshandi, 2020; Das and Chakrabortty, 2021). Seed et al. (1975) proposed the first r_u model for sands which was simplified and modified by many researchers afterward (Booker et al., 1976). Zhang et al. (2021a) predicted a r_u model for fiber-reinforced sands, considering the combined effect of fiber content (FC), fiber length (FL), cyclic stress ratio (CSR), and relative density (D_r). In this study, a r_u model is predicted which depends on FC, and γ. Figure 5.1 (a) shows the excess pore water pressure ratio (r_u) versus cyclic

number ratio (N/N_L) curves at the shear strain rate of 0.6%. The curves can be divided into two sections, i.e., stage 1: where r_u increases vertically almost instantly, and stage 2: where r_u becomes steady and slope increases slowly. The curve depicts an exponential variation, and it is assumed that the fiber-reinforced MSW model can be represented by the following Equation 5.1:

$$r_u = \mathrm{a} - \mathrm{b}c^{\frac{N}{N_L}} \tag{5.1}$$

where a, b, and c are the dimensionless coefficients, r_u is the excess pore water pressure ratio (ratio of excess pore water pressure to initial effective confining pressure) and N/N_L is the cyclic number ratio (ratio of the number of cycles of loading to the number of cycles required for liquefaction). The extensive nonlinear fitting of the test results determines all three unknown coefficients and is shown in Table 5.1, with the range of R^2 values from 0.6 to 0.9.

On further analyzing the Equation 5.1 constants, it can be observed that 'a' is almost constant. To establish r_u model 'a' value can be taken as average (0.951), whereas coefficient 'b' can be related to other parameters of the test, i.e., FC, and γ by introducing another dimensionless parameter 'm' defined as in Equation 5.2:

$$m = \frac{FC}{\gamma} \tag{5.2}$$

where FC is the fiber content (%) and γ is the shear strain (%). Now, let $b=mb_1$, the values of the b_1 (non-dimensional parameter) are also given in Table 5.2, and Equation 5.1 changes to the following Equation 5.3:

$$r_u = 0.951 - \mathrm{m}b_1c^{\frac{N}{N_L}} \tag{5.3}$$

To examine the effectiveness of the above-proposed r_u model for the reinforced MSW fines, the values of $r_{u(model)}$ which is computed through Equation 5.3 are compared

with $r_{u(experimental)}$ for different FC for all three shear strains considered in the study (0.6,0.9, and 1.2%) and are presented in Figure 5.1 (b, c, and d). The model-predicted values agreed satisfactorily with the experimental data. Although this model needs to be refined further as this includes only limited parameters. The effect of σ'_c, f, fiber length, density, etc. has not been considered for this study.

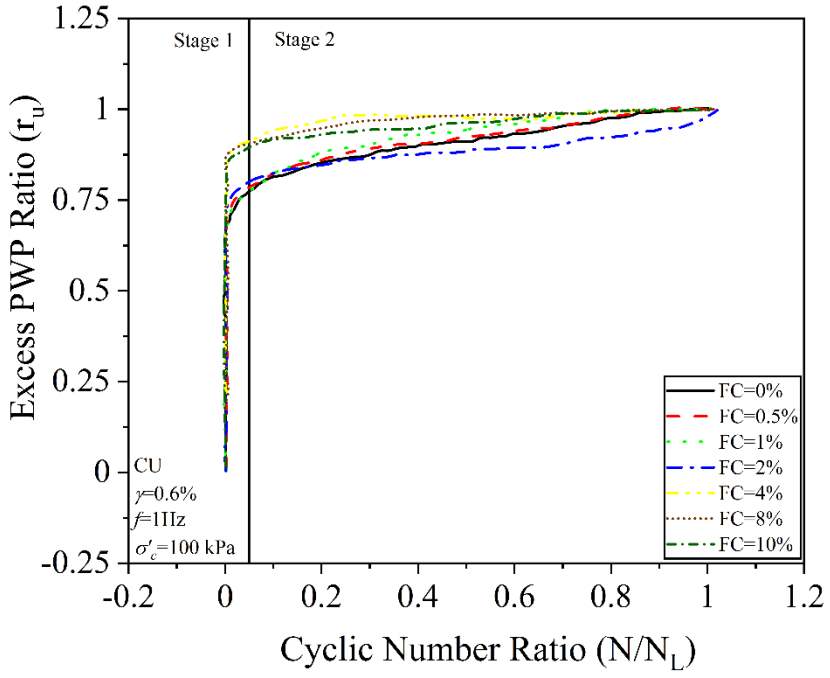

(a)

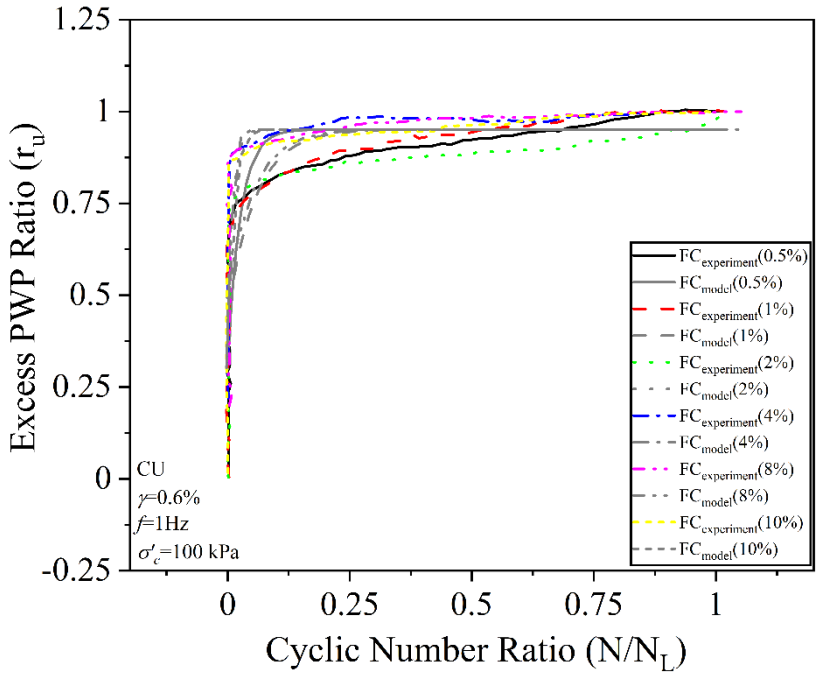

(b)

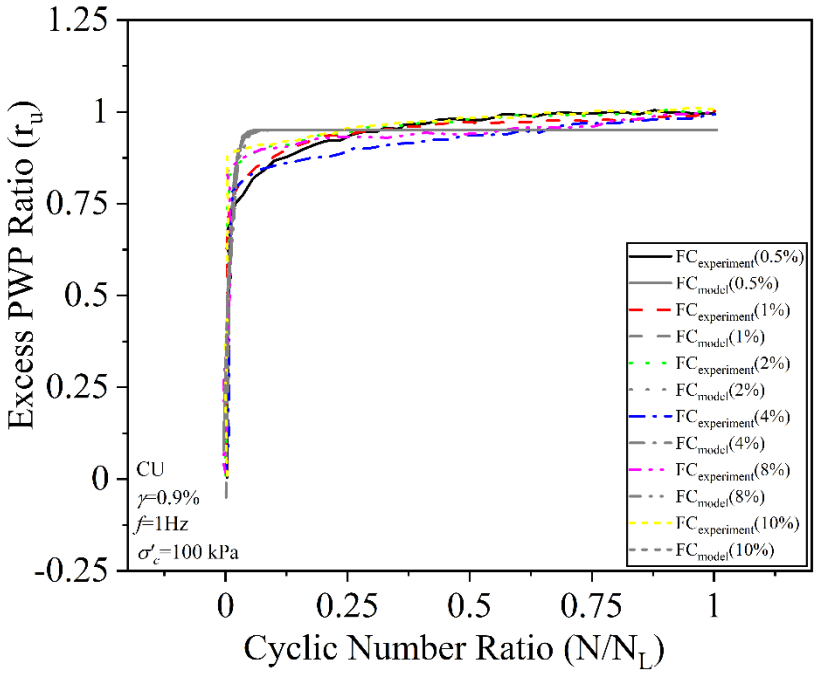

(c)

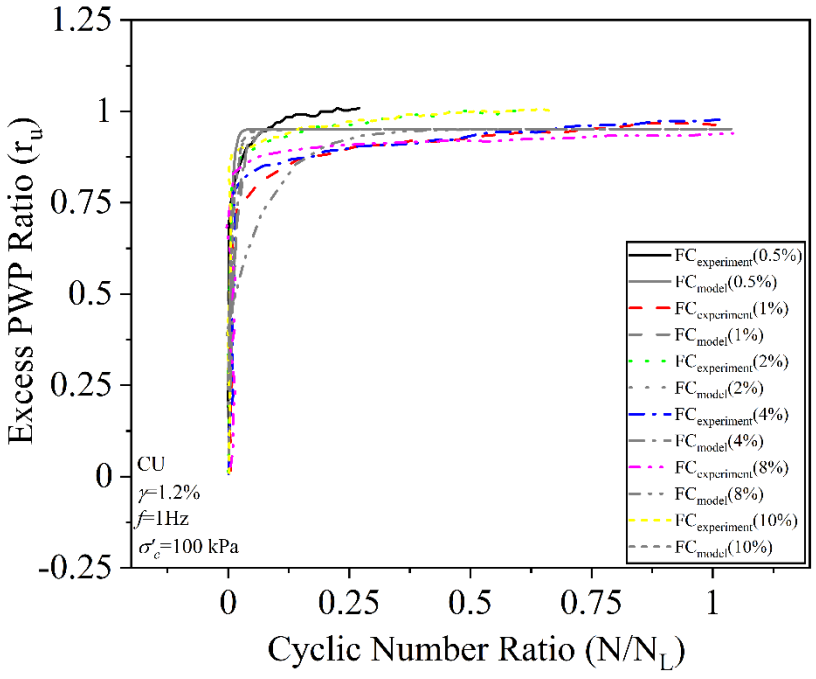

(d)

Figure 5.1 (a) Curves for r_u versus N/N_L (γ=0.6%). Comparisons between experimental and model predicted results for **(b)** γ=0.6%, **(c)** γ=0.9%, and **(d)** γ=1.2%

Table 5.1 Nonlinear fittings for the parameters a, b, b_1, and c used in the r_u (excess pore water pressure ratio) model.

γ (%)	FC (%)	a	b	b_1	c	R^2
0.6	0	0.917 ± 0.019	0.559 ± 0.029	-	1.399E-13 ± 1.009E-12	0.768
0.6	0.5	0.925± 0.019	0.637 ± 0.037	0.765	2.418E-17 ± 2.767E-16	0.797
0.6	1	0.947 ± 0.017	0.502 ± 0.027	0.301	2.708E-8 ± 1.012E-7	0.783
0.6	2	0.894 ± 0.021	0.580 ± 0.054	0.174	9.121E-43 ± 3.137E-41	0.743
0.6	4	0.971 ± 0.018	0.534 ± 0.046	0.080	2.057E-51 ± 8.332E-50	0.816
0.6	8	0.985 ± 0.034	0.445 ± 0.053	0.033	6.369E-9 ± 7.286E-8	0.635
0.6	10	0.960 ± 0.024	0.546 ± 0.052	0.033	1.486E-33 ± 6.018E-32	0.725
0.9	0	0.966 ± 0.024	0.711 ± 0.083	-	1.065E-60 ± 5.878E-59	0.754
0.9	0.5	0.949 ± 0.015	1.021 ± 0.088	1.838	8.487E-51 ± 1.501E-49	0.883
0.9	1	0.948 ± 0.023	0.814 ± 0.072	0.733	1.758E-46 ± 4.035E-45	0.838
0.9	2	0.983 ± 0.019	0.774 ± 0.062	0.348	7.907E-39 ± 1.477E-37	0.865
0.9	4	0.928 ± 0.016	1.112 ± 0.089	0.250	9.860E-47 ± 1.351E-45	0.907
0.9	8	0.952 ± 0.027	0.642 ± 0.053	0.072	5.991E-35 ± 9.529E-34	0.844
0.9	10	0.977 ± 0.025	0.672 ± 0.065	0.060	4.691E-40 ± 1.413E-38	0.764
1.2	0	0.942 ± 0.025	0.742 ± 0.100	-	3.684E-56 ± 1.888E-54	0.779
1.2	0.5	0.963 ± 0.020	0.738± 0.065	1.771	2.005E-72 ± 9.051E-71	0.828
1.2	1	0.930 ± 0.027	0.950 ± 0.148	1.140	7.302E-32 ± 1.772E-30	0.849
1.2	2	0.975 ± 0.018	0.732 ± 0.048	0.439	2.861E-45 ± 5.684E-44	0.914
1.2	4	0.933 ± 0.016	0.989 ± 0.074	0.297	2.239E-36 ± 2.360E-35	0.901
1.2	8	0.958 ± 0.034	0.542 ± 0.065	0.081	3.980E-6 ± 2.862E-5	0.655
1.2	10	0.975 ± 0.024	0.726 ± 0.085	0.087	5.658E-48 ± 2.081E-46	0.750

5.3 CORRELATION BETWEEN SMALL STRAIN SHEAR MODULUS (G_{max}) WITH SHEAR STRENGTH (τ) FOR FIBER REINFORCED MSW FINES

All the test results were considered for the correlation study between the small-stain shear modulus (G_{max}) obtained from the bender element analysis and the shear strength (τ) obtained from the triaxial test under UU (unconsolidated undrained) conditions considering unreinforced (UR) and fiber reinforced (R) MSW fines at a fixed density of 1.51g/cc (MDD). The G_{max} and τ values were normalized by taking the ratio of G_R/G_{UR} and τ_R/τ_{UR}, where G_R is the maximum shear modulus for fiber-reinforced MSW fines with different FC; G_{UR} is the maximum shear modulus for unreinforced MSW fines; τ_R is the maximum shear strength for fiber-reinforced MSW fines with different FC; τ_{UR} is maximum shear strength for fiber unreinforced MSW fines. Each data set consists of G_R/G_{UR} and τ_R/τ_{UR} values for every considered FC (0,0.5,1,2,4,8, and 10%) for different f (0.25,0.5,0.75,1, and 1.5 kHz) and σ_c (50, 100, and 150 kPa) (Figure5.2). The cubic polynomial non-linear model fits well with each data set and can be confirmed through the R^2 values which range from 0.7 to 0.99. Equation 5.4 defines the cubic polynomial model.

$$y = A + B * (x) + C * (x)^2 + D * (x)^3 \tag{5.4}$$

where, y is the independent variable G_R/G_{UR} and x is dependent $\tau_R/\tau_{UR,}$ and A, B, C, and D are the constants. The values of the constants are defined in Table 5.2. Equation 5.4 can be written as Equation 5.5.

$$G_R/G_{UR} = A + B * \left(\frac{\tau_R}{\tau_{UR}}\right) + C * \left(\frac{\tau_R}{\tau_{UR}}\right)^2 + D * \left(\frac{\tau_R}{\tau_{UR}}\right)^3 \tag{5.5}$$

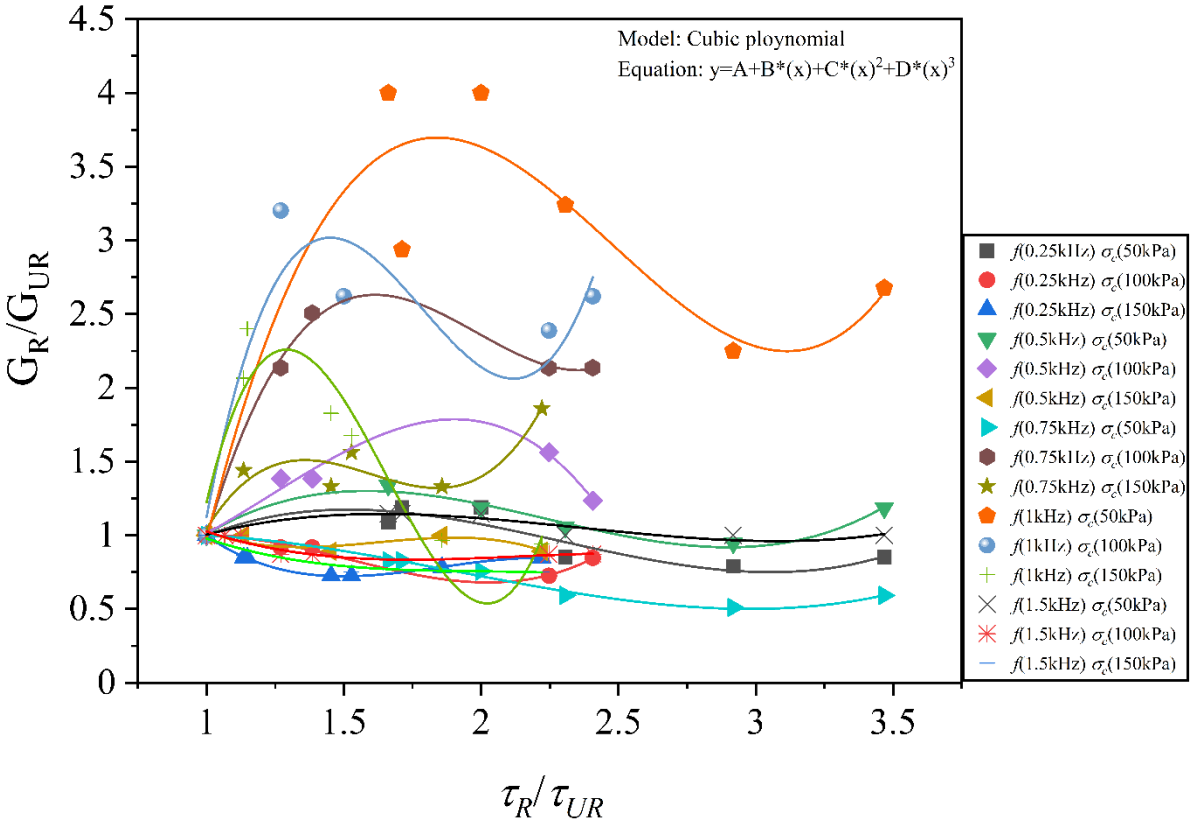

Figure 5.2 Correlation between G_R/G_{UR} and τ_R/τ_{UR}

Table 5.2 Nonlinear fittings for the parameters A, B, C, and D used in the cubic polynomial model.

S.No.	f (kHz)	σ_c (kPa)	A	B	C	D	R^2
1	0.25	50	-0.88 ± 0.89	3.25 ± 1.36	-1.60 ± 0.66	0.23± 0.10	0.81
2	0.25	100	-0.52 ± 0.92	3.61± 1.85	-2.69 ± 1.19	0.59 ± 0.24	0.97
3	0.25	150	4.79± 0.22	-7.03 ± 0.45	3.94 ± 0.28	-0.71 ± 0.05	0.99
4	0.5	50	-1.69 ± 0.41	4.62 ± 0.65	-2.25± 0.32	0.33 ± 0.04	0.96
5	0.5	100	1.41 ± 2.6	-2.67 ± 5.24	3.12 ± 3.39	-0.84 ± 0.69	0.95
6	0.5	150	3.85± 2.42	-5.71± 4.86	3.62 ± 3.12	-0.74± 0.64	0.70
7	0.75	50	0.70 ± 0.28	0.79 ± 0.36	-0.59 ± 0.17	0.10 ± 0.02	0.98
8	0.75	100	-15.29± 2.32	28.80 ± 4.68	-15.04 ± 3.02	2.5 ± 0.62	0.99
9	0.75	150	-11.43 ± 5.52	25.29 ± 11.15	-16.19 ± 7.20	3.37 ± 1.49	0.88
10	1	50	-14.12 ± 4.36	24.11 ± 6.91	-10.42 ± 3.38	1.40 ± 0.51	0.87
11	1	100	-30.12 ± 18.56	59.22 ± 37.16	-34.39 ± 23.78	6.42± 4.83	0.84
12	1	150	-32.78 ± 11.01	68.95 ± 22.07	-43.75± 14.20	8.80 ± 2.93	0.85
13	1.5	50	-0.11 ± 0.38	1.86 ± 0.60	-0.87± 0.29	0.12± 0.044	0.83
14	1.5	100	2.44 ± 0.93	-2.39 ± 1.87	1.16 ± 1.21	-0.18 ± 0.24	0.87
15	1.5	150	2.42 ± 2.21	-2.46 ± 4.46	1.22 ± 2.88	-0.20 ± 0.59	0.84

5.4 PREDICTION MODEL FOR DISSIPATED ENERGY OF UNREINFORCED AND REINFORCED MSW FINES AT LIQUEFACTION

5.4.1 Energy Method

Nemat-Nasser and Shokooh (1979) proposed the energy-based approach for the evaluation of liquefaction as an alternative to the stress-based approach. In comparison to stress and strain-based approaches, the primary benefits of the energy-based method are: (1) energy is a scalar quantity that encompasses the entire spectrum of the ground motion into consideration (Baziar et al., 2011; Baziar and Jafarian, 2007), (2) the application of the energy approach allows for the inclusion of strain, stress, and material properties to the examination of liquefaction (Liang, 1995; Law, 1990). The energy method primarily includes the fundamental components of the approaches based on stress and deformation in the formulation. The area of the hysteresis loop (obtained from the strain-controlled cyclic simple shear test) defines the energy of each loading cycle (Ostadan et al., 1996). The area of the hysteresis loop also defines the dissipated energy per unit volume of the groundmass (Green, 2001). From the dynamic test data up to the onset of liquefaction, the instantaneous energy, and the sum of this energy for the given time intervals can be calculated. The sum of this calculated energy is used to determine the soil mass energy capacity against liquefaction. The capacity energy is a good way to assess the liquefaction because it is affected by shear stress and shear deformation during cyclic loading.

A typical plot of the dissipated energy/unit volume for each cycle until liquefaction for MSW fines sample at relative compaction of 90%, confining pressure 100 kPa, loading frequency 1Hz, and shear strain of 1.5% is shown in Figure 5.3. The progression of loading cycles until liquefaction results in a decrease in the area of the hysteresis loop, which tends to become flat at the end. This indicates that the amount of dissipated energy decreases as

the loading cycle progresses due to the increase in the pore pressure generation under undrained conditions. This was due to the decrease in resistance of the specimen against deformation. The specimen derives its strength from the inter-particle resistance, which decreases with the increase in the pore pressure and, as a result, the effective stress decreases, resulting in liquefaction of the material. It can also be observed that the dissipation of energy in the first few cycles is much high, which was decreased in the later cycles. Figure 5.4 depicts a typical representation of the cumulative energy dissipated until the specimen liquefies for the MSW fines sample at relative compaction of 90%, confining pressure of 100 kPa, loading frequency 1Hz, and shear strain of 1.5%. The effect of all four considered parameters (relative compaction, effective confining pressure, loading frequency, shear strain) on the cumulative dissipated energy of the sample at liquefaction can be seen in Figure 5.5 plotted between cumulative dissipated energy (ΔW) and cyclic shear strain (γ). It can be observed that the energy required to liquefy increases with the increase in relative compaction (90 to 98%) and effective confining pressure (50, 70, and 100 kPa), whereas the energy reduces with shear stain increment from 0.6 to 1.5% keeping all other parameters constant. The effect of frequency can be seen as very random, and no conclusion can be predicted about the effect of frequency on the cumulative dissipated energy of MSW fines.

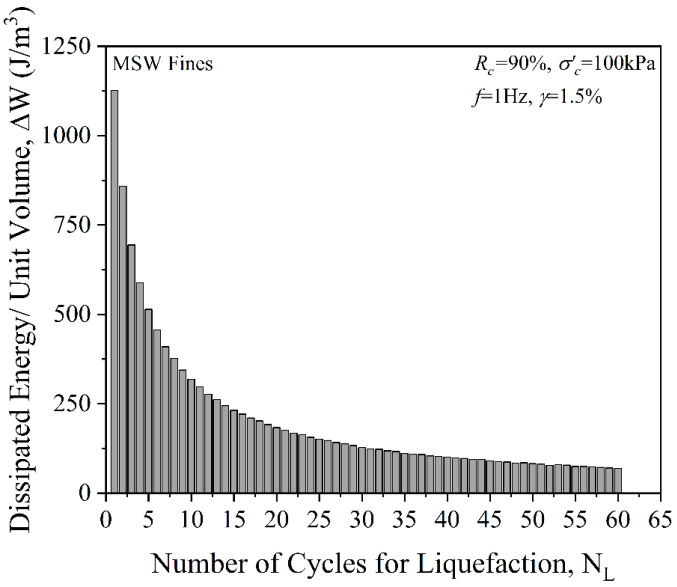

Figure 5.3 Typical variation of dissipated energy/unit volume per cycle until liquefaction of MSW fines sample at R_C=90% tested at f=1 Hz, γ=0.6% and σ'_c=100 kPa

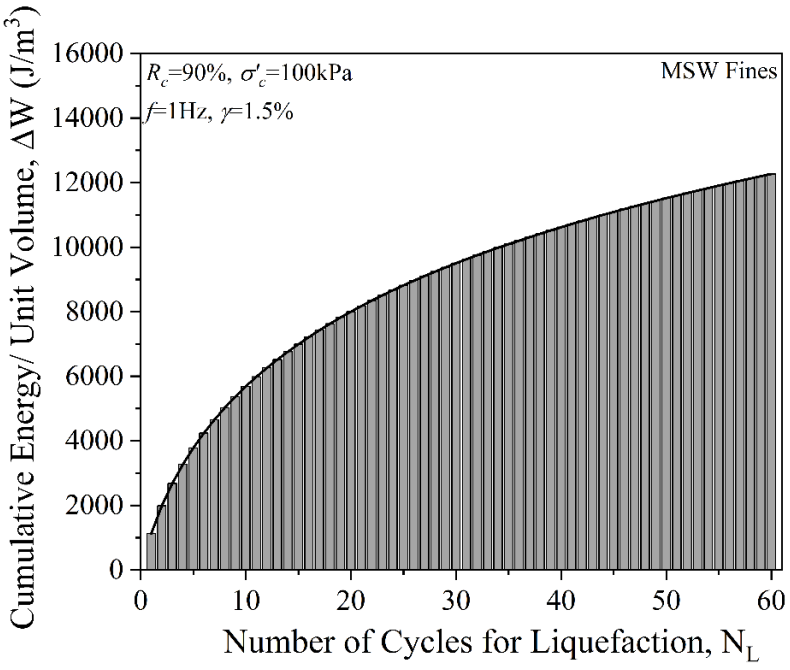

Figure 5.4 Typical variation of cumulative energy/unit volume per cycle until liquefaction of MSW fines sample at R_C=90% tested at f=1 Hz, γ=0.6% and σ'_c=100

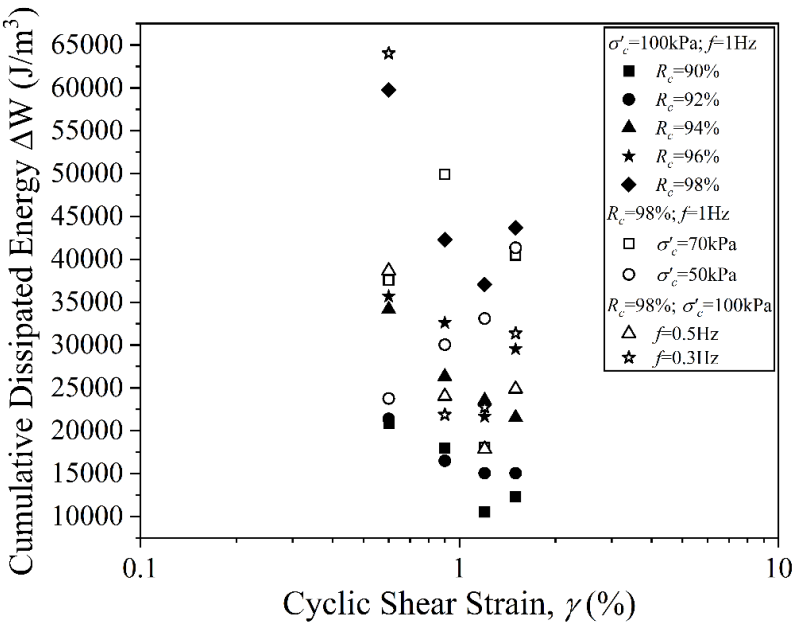

Figure 5.5 Variation of cumulative dissipated energy with cyclic shear strain (γ) of MSW fines specimen representing effect of relative compaction (90 to 98%), effective confining pressure (50 kPa, 70 kPa and 100 kPa), loading frequency (1 Hz, 0.5 Hz and 0.3 Hz)

5.4.2 Linear Regression Model for Dissipated Energy of Unreinforced MSW Fines at Liquefaction

A linear regression model was fitted for the data presented in Figure 5.5 considering the effect of all the parameters on the cumulative dissipated energy of the sample at liquefaction. The dissipated energy for triggering liquefaction is considered as the dependent variable and the relative compaction (R_c), effective confining pressure (σ'_c), cyclic shear strain (γ), and loading frequency (f) are considered as the independent variables. The three equations were developed first considering all four parameters (Equation 5.6), second considering three parameters (except frequency as it is the least affecting parameter) (Equation 5.7), and third considering two parameters (R_c and γ) (Equation 5.8).

$$\log\Delta W = -1.354 + 0.057R_c + 0.002\sigma'_c - 0.154\gamma + 0.246f \quad (5.6)$$

$$\log\Delta W = -1.386 + 0.06R_c + 0.003\sigma'_c - 0.121\gamma \quad (5.7)$$

$$\log\Delta W = 0.99 + 0.06R_c - 0.022\gamma \quad (5.8)$$

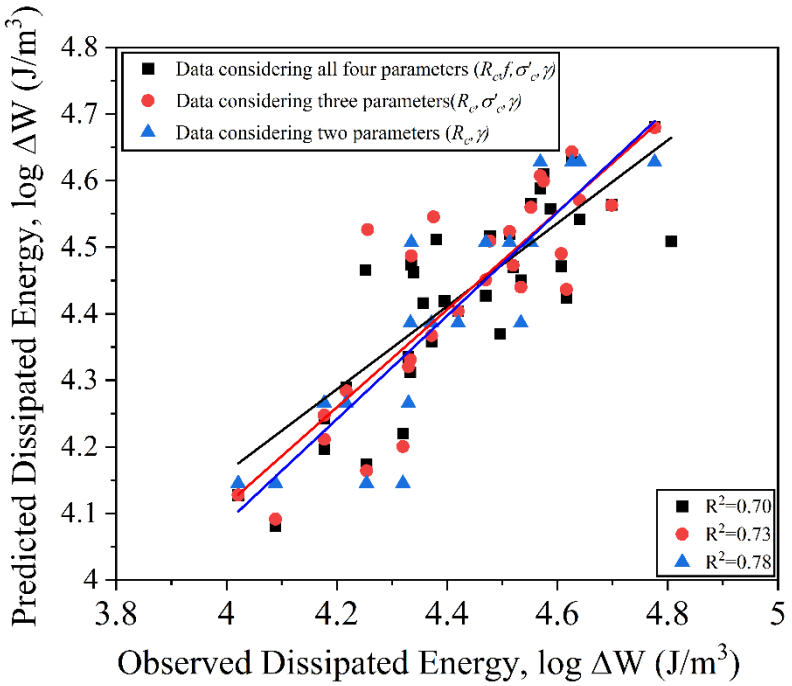

Figure 5.6 Variation of predicted values of dissipated energy of MSW fines with the observed experimental results

Figure 5.6 depicts the variation between the observed and predicted results obtained from the experimental tests using equations 5.6 to 5.8. The R^2 values for all three equations (Equation 5.6 (0.7), Equation 5.7 (0.73), and Equation 5.8 (0.78)) are also mentioned in Figure 5.6. By comparing the R^2 values, the model fits better for Equation 5.8 when two parameters, i.e., relative compaction and shear strain have been considered as these two parameters highly influence the energy dissipation of MSW fines at liquefaction.

5.4.3 Non-Linear Regression Model for Dissipated Energy of Reinforced MSW Fines at Liquefaction

The regression analysis of the fiber-reinforced MSW fines includes only two parameters, i.e., cyclic shear strain (γ) and fiber content (FC). The distribution of dissipated energy at liquefaction with the other two parameters (γ, FC) can be observed in Figure 5.7.

The distribution of data is very random to predict any model although with an increase in shear strain, the dissipated energy at liquefaction slightly decreases.

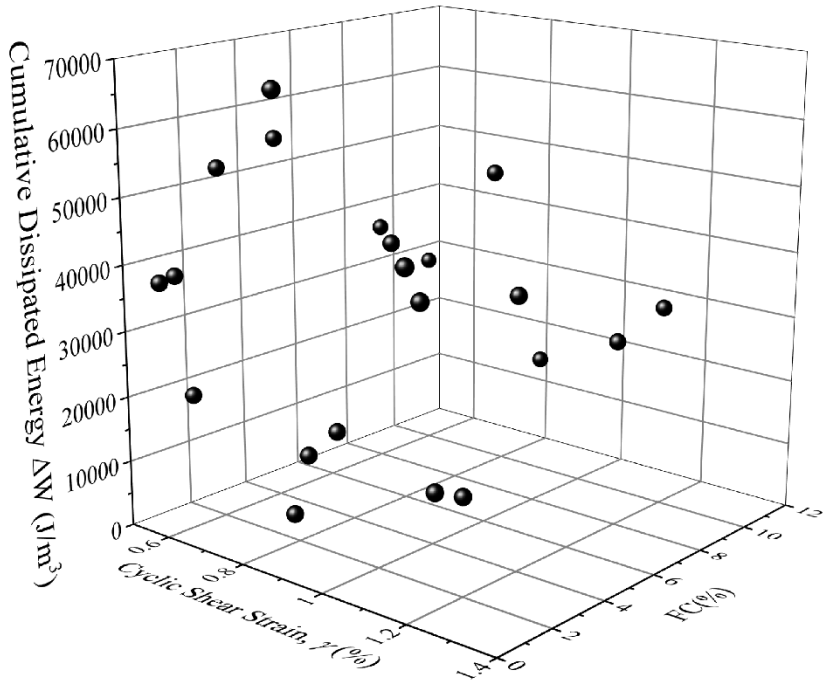

Figure 5.7 Variation of cumulative dissipated energy with cyclic shear strain (γ) and fiber content (FC)

The linear regression model for predicting the dissipated energy of the unreinforced MSW fines does not fit the fiber-reinforced MSW fines data. A new non-linear model is proposed considering two normalized factors, i.e., normalized cumulative dissipated energy ($\Delta W_R/\Delta W_{UR}$) and a factor 'm' (FC/γ) which has been already considered in Equation 5.2. The plot between the two normalized factors can be seen in Figure 5.8. Equation 5.9 below shows the fitted power model between the two factors with R^2 value of 0.74.

$$\Delta W_R/\Delta W_{UR} = 0.38 * (m - 0.51)^{0.33} \quad (5.9)$$

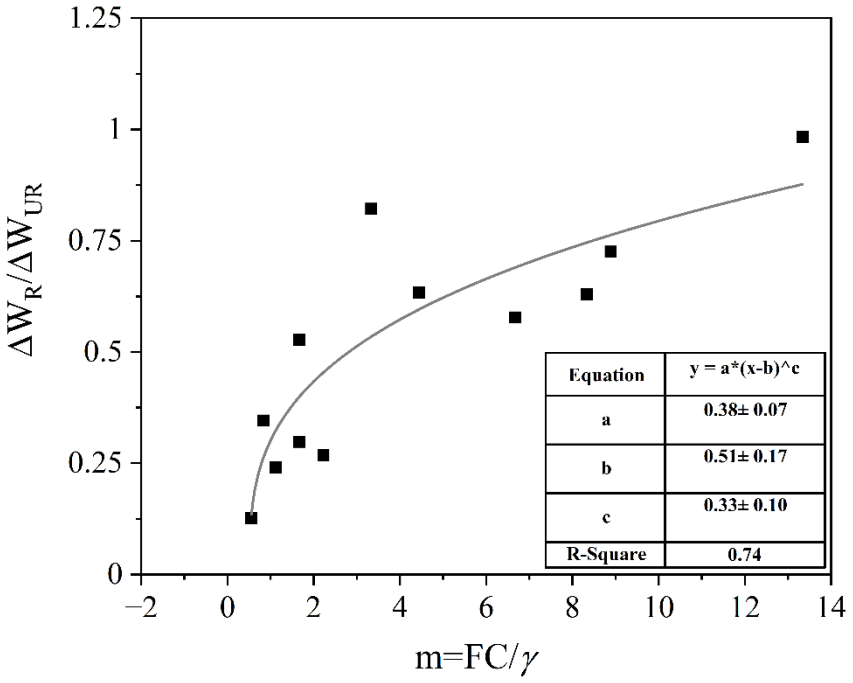

Figure 5.8 Variation of normalised cumulative dissipated energy ($\Delta W_R/\Delta W_{UR}$) with normalised factor 'm' (FC/γ)

5.5 CORRELATIONS BETWEEN NORMALIZED SHEAR MODULUS AND CYCLIC SHEAR STRAIN OF UNREINFORCED AND REINFORCED MSW FINES

The variation of the normalized shear modulus (G/G_{max}) with shear strain is an important input parameter in the dynamic response analysis of soil and solid waste landfills. Based on the experimental data, Zekkos (2005) proposed a hyperbolic model (Equation 5.10) for calculating the shear modulus for confining stresses ranging from 25 to 90 kPa, for three different waste compositions, i.e., waste containing 100% particles less than 20 mm in size, waste containing 62-76% particles less than 20 mm size, and waste containing 8- 25% particles less than 20 mm size. The a and b values for the three different wastes were (0.118, 0.265, 0.697) and (0.886, 0.819, 0.925) respectively with R^2 values of about 0.9.

$$\frac{\mathrm{G}}{\mathrm{G_{max}}} = \frac{1}{1+(\frac{\gamma}{a})^b} \tag{5.10}$$

However, the above-presented hyperbolic or universal model was not fit well for the data obtained from the present study. Hence, another hyperbolic equation proposed by Choudhury and Savoikar (2009) (Equation 5.11) for MSW was used to fit the present experimental data.

$$\frac{\mathrm{G}}{\mathrm{G_{max}}} = \frac{1}{1+(a*(\gamma)^b)} \tag{5.11}$$

The unreinforced MSW fines data obtained through the cyclic triaxial test was categorized under five relative compactions (R_c) and five different plots were made for the correlations. The strain-dependent normalized shear modulus (G/G_{max}) can be obtained through Equation 5.11 with a and b as hyperbolic model parameters for different R_c (90 to 98%) (Table 5.3). The R^2 value ranges from 0.66 to 0.81 for the five considered densities shown in Figure 5.9.

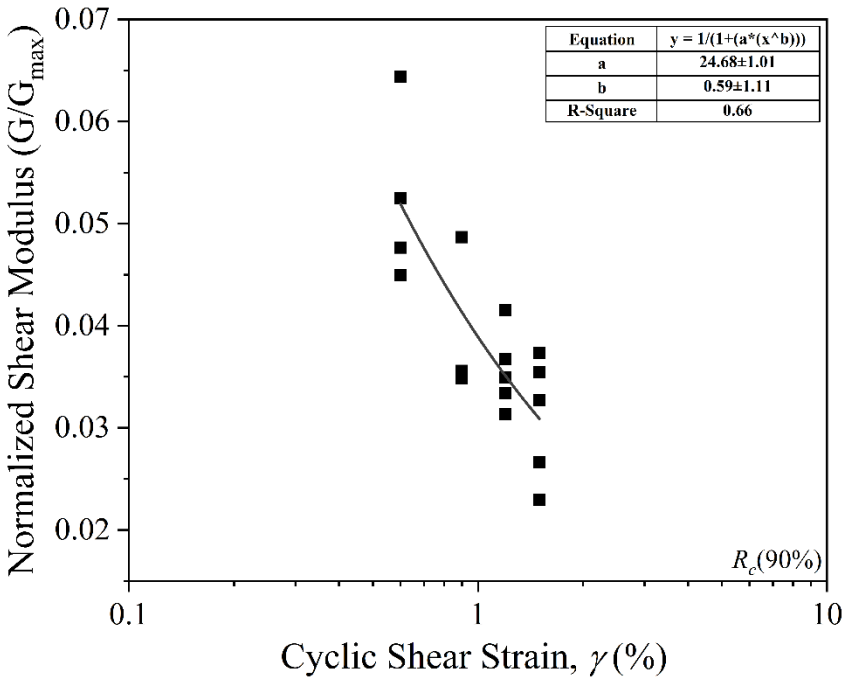

(a)

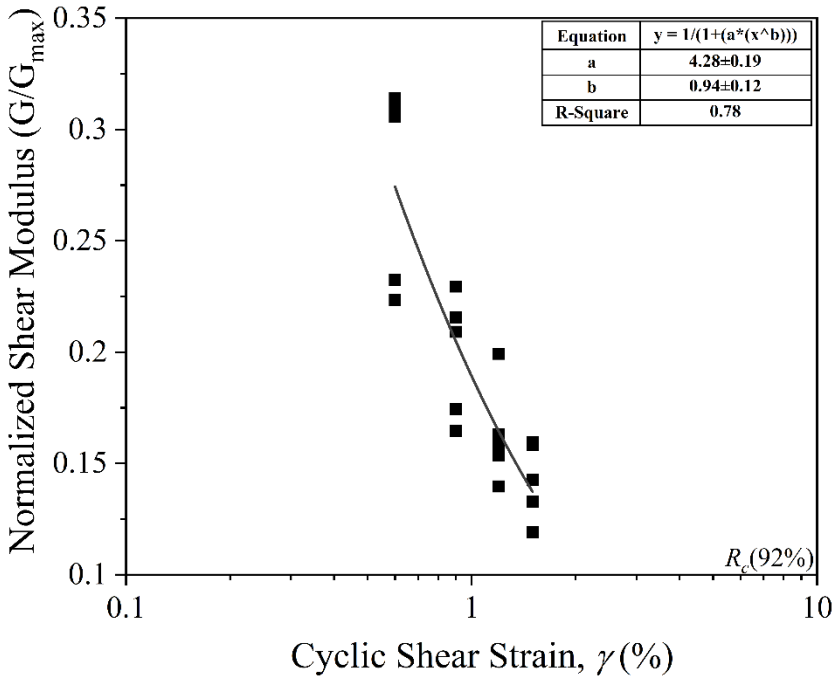
Equation | y = 1/(1+(a*(x^b)))
a | 4.28±0.19
b | 0.94±0.12
R-Square | 0.78
Normalized Shear Modulus (G/G_max)
0.35
0.3
0.25
0.2
0.15
0.1
0.1
1
10
R_c(92%)
Cyclic Shear Strain, γ(%)

(b)

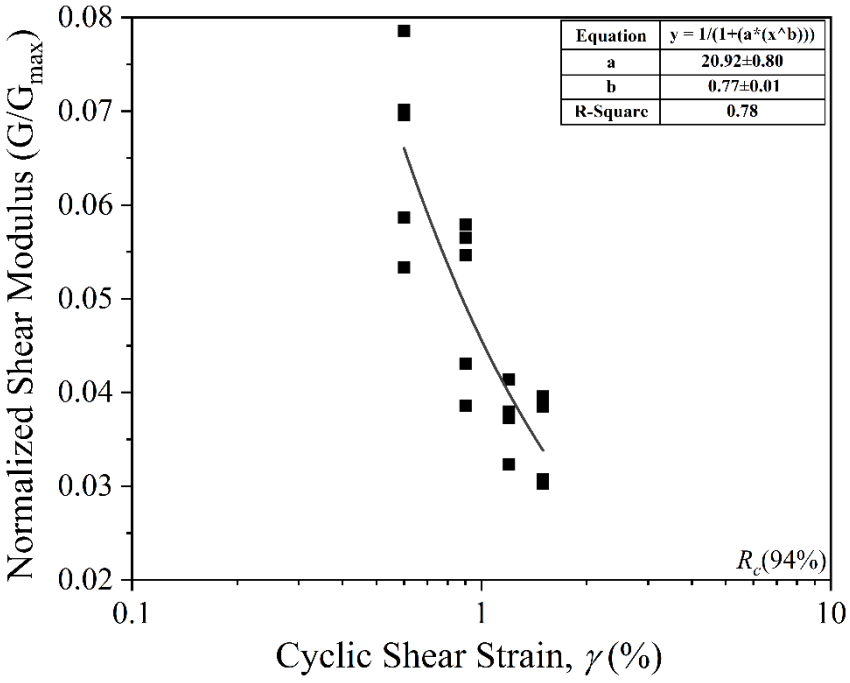
Equation | y = 1/(1+(a*(x^b)))
a | 20.92±0.80
b | 0.77±0.01
R-Square | 0.78
Normalized Shear Modulus (G/G_max)
0.08
0.07
0.06
0.05
0.04
0.03
0.02
0.1
1
10
R_c(94%)
Cyclic Shear Strain, γ(%)

(c)

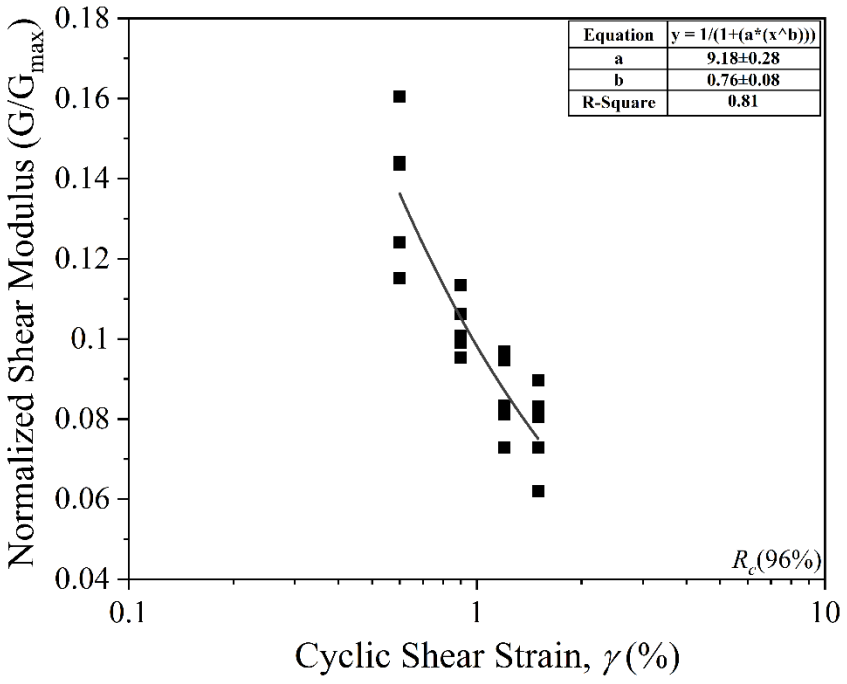

(d)

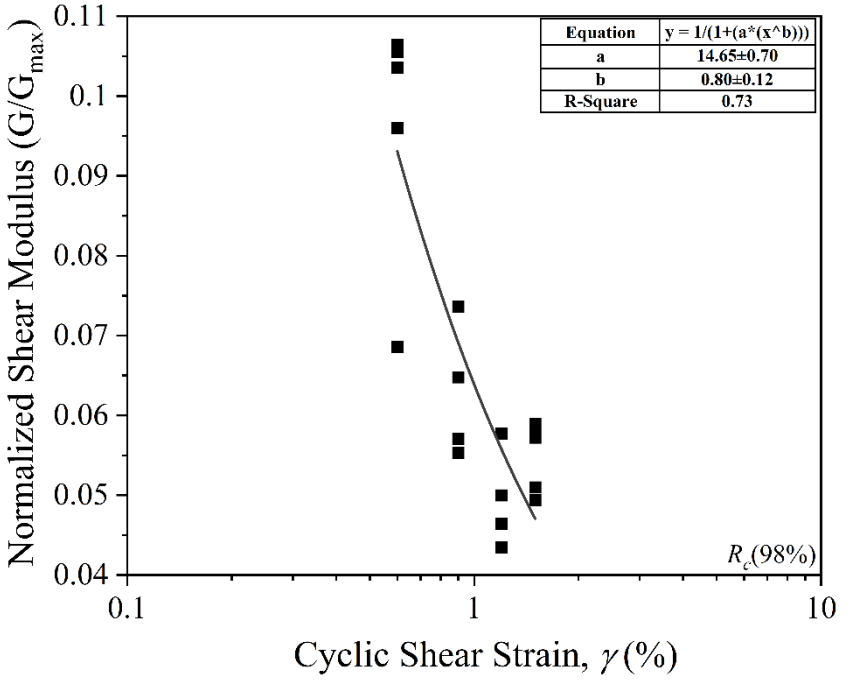

(e)

Figure 5.9 Correlation plot of G/G_{max}– log γ for MSW fines (considering the loading frequency (0.3, 0.5, and 1Hz) and effective confining pressure (50, 70, and 100 kPa) at relative compaction of **(a)** 90% **(b)** 92% **(c)** 94% **(d)** 96% and **(e)** 98%

Table 5.3 Hyperbolic model parameters and R^2 values for the fitted normalized shear modulus (G/G_{max}) vs. log γ correlation at different R_c.

R_c (%)	a	b	R^2
90	24.68	0.59	0.66
92	4.28	0.94	0.78
94	20.92	0.77	0.78
96	9.18	0.76	0.81
98	14.65	0.8	0.73

The data of the fiber-reinforced MSW fines obtained from the unconsolidated undrained cyclic triaxial test has been very limited as it has been performed on fixed density (1.51g/cc), effective confining pressure (100 kPa), and loading frequency (1Hz). The above-used model for the unreinforced MSW fines does not fit well with the provided data set based on R^2 value of 0.5. A new correlation for G/G_{max}- log γ was developed for the fiber-reinforced data set shown in Equation 5.12.

$$\frac{\mathrm{G}}{\mathrm{G_{max}}} = \frac{a*\gamma}{(b+\gamma)} \tag{5.12}$$

In the above model, a and b are the model constants having values 0.073 and -0.39 respectively with R^2 value of 0.96. The correlation for G/G_{max}– log γ for fiber-reinforced MSW fines can be seen in Figure 5.10. The final equation can be written as below (Equation 5.13).

$$\frac{\mathrm{G}}{\mathrm{G_{max}}} = \frac{0.073*\gamma}{(\gamma-0.39)} \tag{5.13}$$

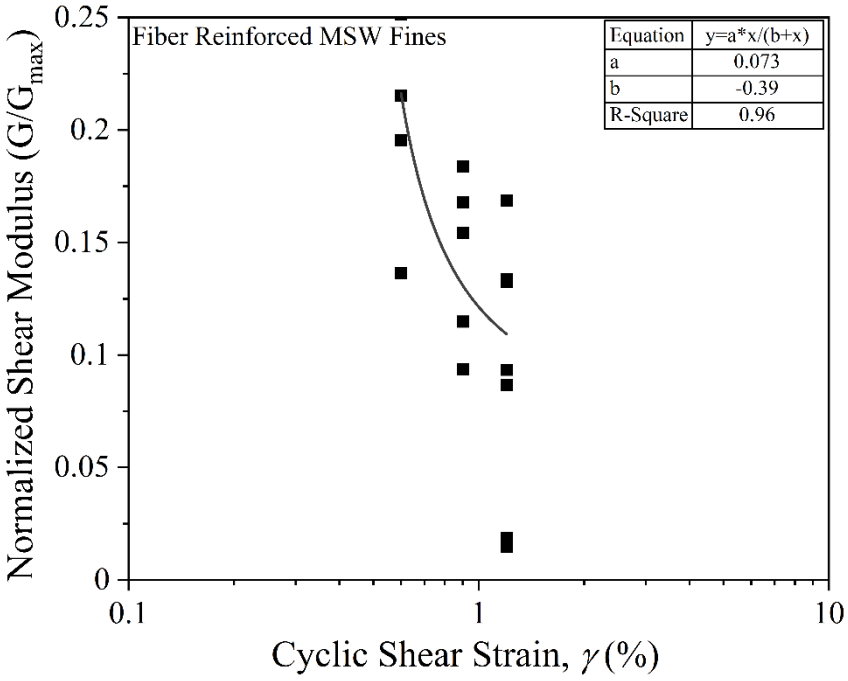

Figure 5.10 Correlation plot of G/G_{max}– log γ for fiber-reinforced MSW fines (considering the loading frequency of 1Hz, effective confining pressure of 100 kPa and density of 1.51g/cc at all the fiber content (0 to 10%)

5.6 CORRELATIONS BETWEEN DAMPING RATIO AND CYCLIC SHEAR STRAIN OF UNREINFORCED AND REINFORCED MSW FINES

The unreinforced MSW fines data obtained through the cyclic triaxial test was categorized under five relative compactions (R_c) and five different plots were made to obtain the correlations between the damping ratio (D) and cyclic shear stain (γ). The correlations were proposed using the model given by Choudhury and Savoikar (2009) as shown below (Equation 5.14).

$$D = 30(1 - e^{c\gamma^d}) \quad (5.14)$$

The two model constants (c and d) values are provided in Table 5.4 with their R^2 values almost equal to 0.7 for every R_c. The five plots of correlations between D– log γ for every considered R_c (90 to 98%) have been shown in Figure 5.11. Each plot consists of the data at one relative compaction for three different frequencies (0.3, 0.5, and 1Hz) and effective confining pressure (50, 70, and 100 kPa).

Table 5.4 Model parameters and R^2 values for the fitted damping ratio vs. shear strain correlation at different R_c.

R_c (%)	c	d	R^2
90	-1.5	-1.02	0.7
92	-1.33	-0.63	0.7
94	-1.7	-1.14	0.75
96	-1.28	-1.21	0.7
98	-1.42	-1.04	0.73

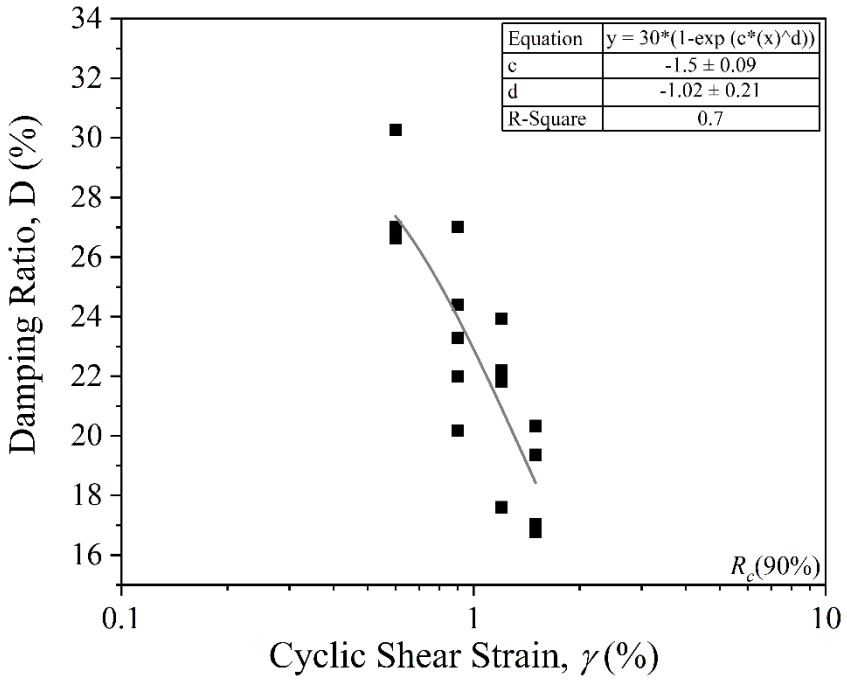

(a)

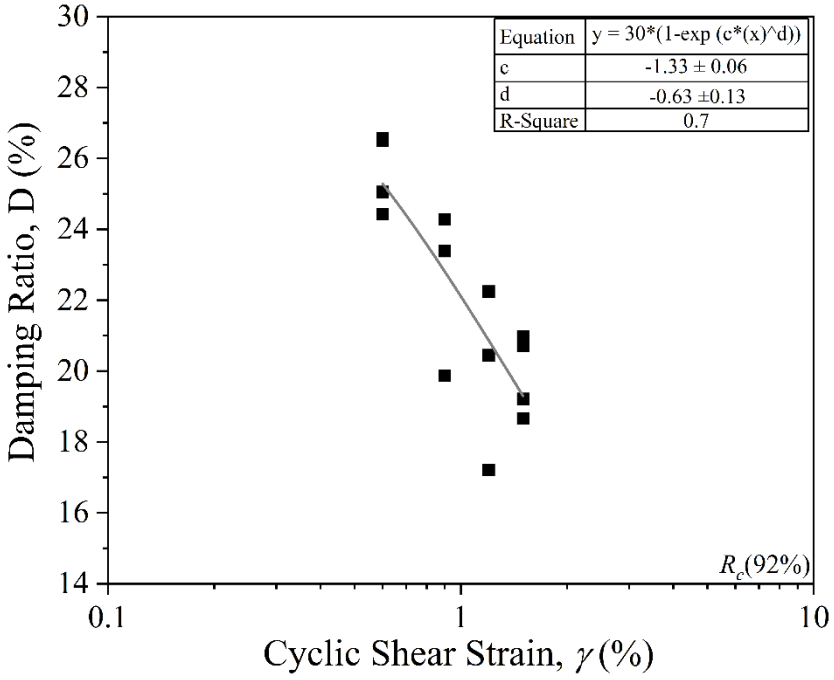
Equation | y = 30*(1-exp (c*(x)^d))
c | -1.33 ± 0.06
d | -0.63 ±0.13
R-Square | 0.7
R_c(92%)
Damping Ratio, D (%)
Cyclic Shear Strain, γ(%)
30
28
26
24
22
20
18
16
14
0.1
1
10

(b)

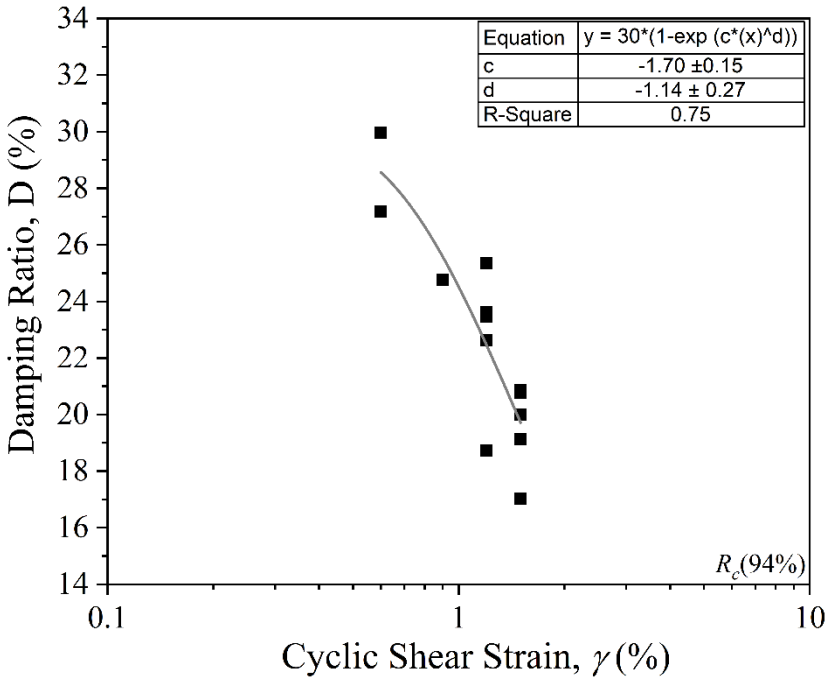
Equation | y = 30*(1-exp (c*(x)^d))
c | -1.70 ±0.15
d | -1.14 ± 0.27
R-Square | 0.75
R_c(94%)
Damping Ratio, D (%)
Cyclic Shear Strain, γ(%)
34
32
30
28
26
24
22
20
18
16
14
0.1
1
10

(c)

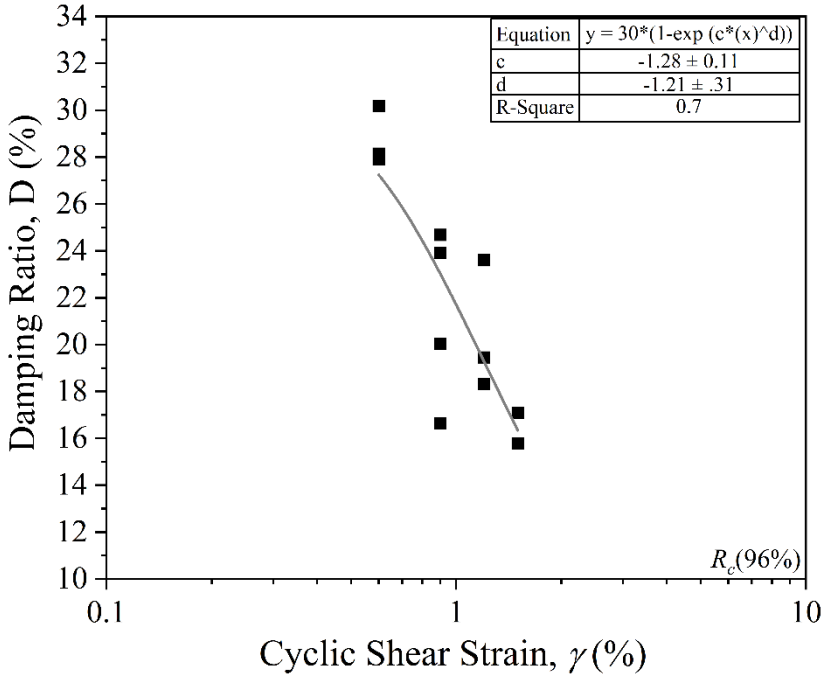

(d)

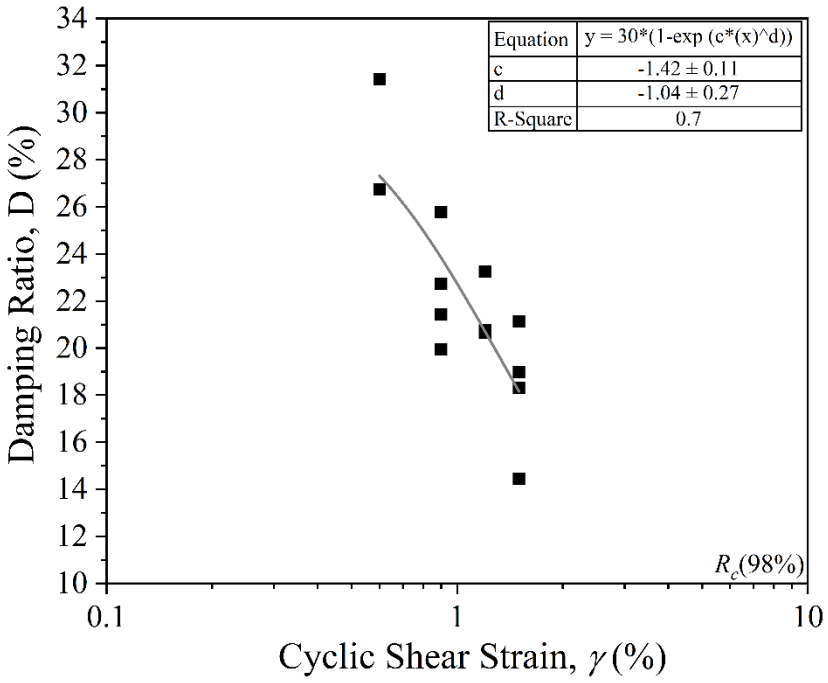

(e)

Figure 5.11 Correlation plot of D– log γ for MSW fines (considering the loading frequency (0.3, 0.5, and 1Hz) and effective confining pressure (50, 70, and 100 kPa) at relative compaction of **(a)** 90% **(b)** 92% **(c)** 94% **(d)** 96% and **(e)** 98%

The above model was applied for the fiber-reinforced MSW fines but the model was not fitting well as the R^2 value obtained was less than 0.5. Another correlation equation was developed for the fiber-reinforced MSW fines using Equation 5.15 with a better R^2 value of 0.6 (Figure 5.12).

$$D = 20 + \frac{30}{1+(\frac{\gamma}{0.83})^{3.3}} \tag{5.15}$$

The limited set of data on the fiber-reinforced MSW fines does not justify the predicted model, hence, additional data may require for better prediction of the model.

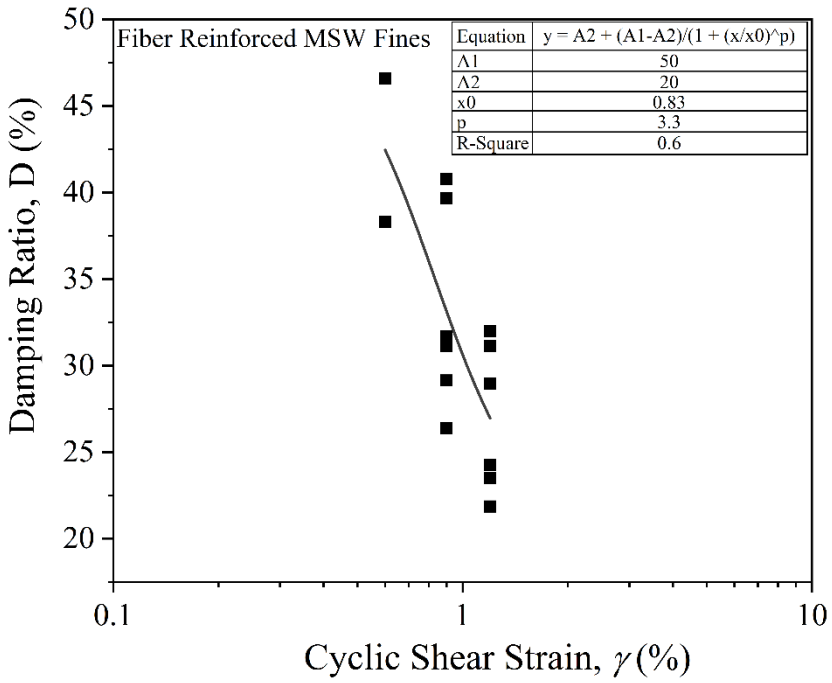

Figure 5.12 Correlation plot of D– log γ for fiber reinforced MSW fines (considering the loading frequency of 1Hz, effective confining pressure of 100 kPa and density of 1.51g/cc at all the fiber content (0 to 10%)

5.7 LIMITATIONS OF THE PRESENTED CORRELATIONS

The present correlations can't be used for MSW fines from any source as the properties of the waste change from place to place and the material itself is heterogeneous even on the micro-scale. The correlations are developed for the reconstituted samples of unreinforced or reinforced MSW fines at a specific density, so these correlations can't be used for any sample directly collected from the field. Only a particular segregated portion of the MSW, i.e., particles less than 4.75 mm has been considered for the study, so it is difficult to compare it with the field landfill data. The number of data set is also comparatively low to predict any universal model for the material. These correlation models can be used to predict the general seismic behaviour of this material and with future advanced studies, these models can be improved.

5.8 SUMMARY

To develop the empirical correlations for the unreinforced and fiber-reinforced MSW fines almost 100 cyclic triaxial test results on the unreinforced MSW fines and 21 on the fiber-reinforced MSW fines data were considered. To analyze the seismic performance of any material (soil/waste), it is required to have the stiffness and damping properties of the considered material so that further numerical modeling and seismic behaviour of the material can be predicted under any dynamic loading conditions due to any natural or unnatural sources. Other than dynamic properties, the pore water pressure dissipation and its model with liquefaction cycles help to understand the liquefaction behaviour of the material (unreinforced and reinforced MSW fines). The liquefaction potential can also be predicted through the dissipated energy model, which provides a better

representation of failure in terms of energy. The small-strain shear modulus (G_{max}) is also a very important parameter required to obtain the normalized strain-dependent modulus reduction (G/G_{max}) curve and its correlation with a static shear strength of reinforced MSW fines can help to predict the G_{max} in the absence of data. These correlations can be useful for dynamic response analyses of structures made of unreinforced or reinforced MSW fines under seismic or cyclic loading conditions.